

Identification of (*R*)-[¹⁸F]YH134 for Monoacylglycerol Lipase Neuroimaging and Exploration of Its Use for Central Nervous System and Peripheral Drug Development

Yingfang He¹, Stefanie D. Krämer¹, Uwe Grether², Matthias B. Wittwer², Ludovic Collin², Bernd Kuhn², Andreas Topp², Dominik Heer², Fionn O'Hara², Michael Honer², Anto Pavlovic², Hans Richter², Martin Ritter², Didier Rombach², Claudia Keller¹, Luca Gobbi², and Linjing Mu¹

¹Center for Radiopharmaceutical Sciences, Institute of Pharmaceutical Sciences, Department of Chemistry and Applied Biosciences, ETH Zurich, Zurich, Switzerland; and ²Pharma Research and Early Development, Roche Innovation Center Basel, F. Hoffmann-La Roche Ltd., Basel, Switzerland

This study aimed to evaluate (*R*)-[¹⁸F]YH134 as a novel PET tracer for imaging monoacylglycerol lipase (MAGL). Considering the ubiquitous expression of MAGL throughout the whole body, the impact of various MAGL inhibitors on (*R*)-[¹⁸F]YH134 brain uptake and its application in brain–periphery crosstalk were explored. **Methods:** MAGL knockout and wild-type mice were used to evaluate (*R*)-[¹⁸F]YH134 in vitro autoradiography and PET experiments. To explore the impact of peripheral MAGL occupancy on (*R*)-[¹⁸F]YH134 brain uptake, PET kinetics with an arterial input function were studied in male Wistar rats under baseline and blocking conditions. **Results:** In vitro autoradiography, (*R*)-[¹⁸F]YH134 revealed a heterogeneous distribution pattern with high binding to MAGL-rich brain regions in wild-type mouse brain slices, whereas the radioactive signal was negligible in MAGL knockout mouse brain slices. The in vivo brain PET images of (*R*)-[¹⁸F]YH134 in wild-type and MAGL knockout mice demonstrated its high specificity and selectivity in mouse brain. A Logan plot with plasma input function was applied to estimate the distribution volume (V_T) of (*R*)-[¹⁸F]YH134. V_T was significantly reduced by a brain-penetrant MAGL inhibitor but was unchanged by a peripherally restricted MAGL inhibitor. The MAGL target occupancy in the periphery was estimated using (*R*)-[¹⁸F]YH134 PET imaging data from the brain. **Conclusion:** (*R*)-[¹⁸F]YH134 is a highly specific and selective PET tracer with favorable kinetic properties for imaging MAGL in rodent brain. Our results showed that blocking of the peripheral target influences brain uptake but not the V_T of (*R*)-[¹⁸F]YH134. (*R*)-[¹⁸F]YH134 can be used for estimating the dose of MAGL inhibitor at half-maximal peripheral target occupancy.

Key Words: monoacylglycerol lipase; PET imaging; plasma input function; drug occupancy studies

J Nucl Med 2024; 00:1–6

DOI: 10.2967/jnumed.123.266426

Monoacylglycerol lipase (MAGL) is a serine hydrolase that belongs to the endocannabinoid system. It is expressed in various organs, including the brain, heart, liver, kidney, adipose tissue,

and adrenal gland (1,2). MAGL plays a key role in hydrolyzing endocannabinoid 2-arachidonoylglycerol to arachidonic acid, the main precursor for proinflammatory eicosanoids (3,4). The dual role of MAGL in the regulation of neuroinflammation and endocannabinoid signaling makes it a promising therapeutic target for several neurologic disorders. Pharmacologic inhibition of MAGL led to therapeutic effects in animal models of Alzheimer disease (4,5), Parkinson disease (6), and multiple sclerosis (7), as well as psychiatric disorders, among others (8–10). In addition, peripheral MAGL was suggested to serve as a critical hub in lipid signaling under physiologic and oncologic conditions (11,12). Moreover, peripherally restricted MAGL inhibitors may be of use for treatments against metabolic disorders, obesity, and cancer (8).

PET imaging of MAGL enzymes in the central nervous system (CNS) enables precision pharmacology to address elemental questions during drug development (13). A suitable MAGL PET tracer can provide quantitative information about drug–target interactions and facilitate the assessment of target alterations under disease conditions (14,15). So far, [¹⁸F]T-401 has been the only tracer shown capable of visualizing MAGL in the human brain (16). [¹¹C]PF-06809247 revealed promising results in a target occupancy study in the brain of nonhuman primates (17). Recently, we disclosed the discovery of (*R*)-[¹⁸F]YH149 (Fig. 1), an [¹⁸F]T-401 derivative that exhibits improved brain penetration and appropriate clearance from the brain target in vivo (18). However, in subsequent work, a radiometabolite was detected in mouse brain, which complicates quantitative PET and kinetic modeling. This study set out to investigate a novel compound, (*R*)-YH134, the meta-fluorine–substituted analog of (*R*)-[¹⁸F]YH149. In comparison to (*R*)-YH149, (*R*)-YH134 revealed 1.3-fold and 2-fold lower clearance in mouse and human liver microsomes, respectively. This finding suggests an improved stability of (*R*)-YH134 against cytochrome P450 oxidation in phase I metabolism. Further in vivo characterization of (*R*)-[¹⁸F]YH134 (Fig. 1) revealed an improved kinetic profile, particularly regarding the absence of radiometabolites in rodent brain. Encouraged by these promising results, kinetic modeling was performed with an arterial input function (IF). Considering the ubiquitous and high expression of MAGL in the CNS and periphery, we further explored the brain–periphery crosstalk in CNS tracer and drug development, and we attempted to answer the following questions: How does peripheral MAGL inhibition influence brain uptake of (*R*)-[¹⁸F]YH134 for neuroimaging? Can a MAGL CNS PET tracer facilitate the characterization

Received Aug. 3, 2023; revision accepted Nov. 7, 2023.

For correspondence or reprints, contact Linjing Mu (linjing.mu@pharma.ethz.ch).

Published online Dec. 21, 2023.

COPYRIGHT © 2024 by the Society of Nuclear Medicine and Molecular Imaging.

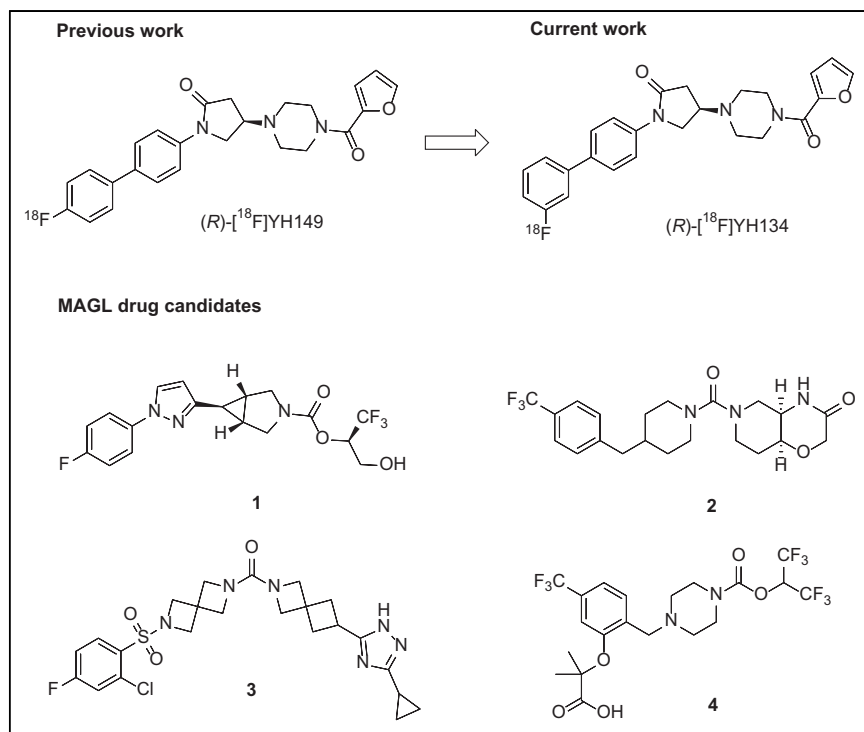


FIGURE 1. Chemical structures of (R) - $[^{18}\text{F}]$ YH149, (R) - $[^{18}\text{F}]$ YH134, and 4 MAGL blockers for in vivo studies.

of peripherally restricted MAGL inhibitors during drug development? As illustrated in Figure 1, 4 MAGL drug candidates were selected for the studies (19–21). The impact of peripheral MAGL inhibition on (R) - $[^{18}\text{F}]$ YH134 brain kinetics was further examined using elevating doses of compound **3** (Fig. 1).

MATERIALS AND METHODS

The study was approved by the institutional review board. All animal studies were conducted in accordance with ARRIVE guidelines (Animal Research: Reporting of In Vivo Experiments) and Swiss animal protection and welfare legislation and were approved by the Veterinary Office of Canton Zurich. MAGL knockout and wild-type mice were from Taconic Biosciences, and Wistar rats were from Charles River. The husbandry of animals was conducted under standard conditions as previously reported (22). The apical efflux ratios from P-glycoprotein (P-gp) of MAGL inhibitors were measured as previously reported (23). A CEREP screen consisting of 50 receptors or enzymes was performed using radioligand binding displacement or enzymic assays (24). The detailed synthetic procedures for (R) -YH134 and its boronic ester precursor are presented in Supplemental Scheme 1, and experimental details on (R) -YH134 plasma protein binding, in vitro autoradiography, and in vivo animal studies can be found in the supplemental data (supplemental materials are available at <http://jnm.snmjournals.org>).

MAGL Inhibition Constants, Radiochemistry, and In Vitro Characterization

The MAGL inhibition constants (half-maximal inhibitory concentrations) of both the (R) - and the (S) -YH134 enantiomers and the microsomal and hepatic clearance of (R) -YH134 in different species were measured as previously reported (22). ^{18}F -labeled YH134 was produced via copper-mediated radiofluorination of the boronic pinacol

ester precursor (25). Lipophilicity and in vitro stability were evaluated according to published procedures (18).

PET Experiments and Biodistribution After Dissection of MAGL Knockout and Wild-Type Mice

MAGL knockout ($n = 4$) or wild-type ($n = 4$) mice were anesthetized with isoflurane for PET/CT (26). Tracer biodistribution was investigated after dissection. Awake MAGL knockout and wild-type mice (4 for each group) were injected intravenously with (R) - $[^{18}\text{F}]$ YH134 (4.32–11.85 MBq, 2.13–2.51 nmol/kg) and euthanized under isoflurane (5%) anesthesia by decapitation at 30 min after injection. The organs of interest were dissected and weighed, and radioactivity was measured in a γ -counter (Wizard; Perkin Elmer). PET and dissection data are reported as SUV and percentage normalized injected dose per gram of tissue, respectively. Mean values are shown with SD.

In Vivo Radiometabolite Analyses and Tracer Plasma-to-Whole-Blood Ratio

The radiometabolite analyses were performed on C57BL/6 mice and Wistar rats. All samples were analyzed by radio-ultra performance liquid chromatography (UPLC; Waters). The mice were injected with 38–81 MBq of (R) - $[^{18}\text{F}]$ YH134 ($n = 2$). Brain and plasma samples were collected at 45 and 90 min after injection. The rats were assigned to a baseline ($n = 2$) or a blockade ($n = 2$) group. The blockade group was pretreated with compound **3** to investigate whether the blocker affected tracer plasma-to-whole-blood distribution and metabolism.

Rat PET Scans Without Arterial IF

PET scans were conducted on anesthetized male Wistar rats (301–355 g) with 8.33–47.90 MBq of (R) - $[^{18}\text{F}]$ YH134 (0.40–4.48 nmol/kg). Under blockade conditions, the animals were pretreated with a 2 mg/kg dose of compound **1**, a 1 mg/kg dose of compound **2**, various doses of compound **3** (1, 3, 5, or 10 mg/kg), or a 3 mg/kg dose of compound **4**. Blood from the rats receiving compound **3** was collected at 100 min after injection on completion of the PET scans, and plasma was separated by centrifugation and stored at -80°C before being analyzed by liquid chromatography tandem mass spectrometry to determine the concentration of compound **3** in plasma.

Rat PET Scans with Arterial IF

PET kinetics with an arterial IF were determined in male Wistar rats (344–427 g; Supplemental Table 1). For the arterial plasma IF, blood activity was determined from an arteriovenous shunt simultaneously with acquisition of the PET data (27). During PET scanning, blood from either the cannulated tail artery (minimally invasive protocol) or a femoral artery (invasive protocol) was guided through a Twilite coincidence counter (Swisstrace) and a peristaltic pump and then was transferred back to a cannulated lateral tail vein or a femoral vein.

Logan Plot Analysis to Determine Distribution Volume (V_T) of Total Tracer

IF was generated from the blood coincidences by correcting the data with a biexponential function describing the plasma-to-whole-blood ratios. The parent tracer was the only detectable radioactivity in rat plasma up to 60 min after injection; no further correction was

therefore required for the IF. V_T was calculated as the slope of the linear part of the Logan plot generated from the IF and the PET data (28).

Statistical Analysis

Data were compared by a homoscedastic, 2-tailed Student's *t* test in Excel (version 2013; Microsoft) or R (version 4.2.2; The R Project for Statistical Computing), assuming equal variance (comparison of 2 conditions) or by ANOVA with post hoc correction for multiple comparisons (the Tukey honestly significant difference test; functions *aov* and *TukeyHSD* in R), as indicated. A *P* value of less than 0.05 was considered statistically significant.

RESULTS

Properties of (R)-YH134

(R)-YH134 exhibited potent inhibition, with a similar half-maximal inhibitory concentration of 11 nM toward mouse and human MAGL enzyme. However, (S)-YH134 showed significant loss of MAGL-inhibiting activity, with half-maximal inhibitory concentrations of 397 nM in mice and 197 nM in humans. The apparent intrinsic clearance of (R)-YH134 was determined as 93, 71, and 10 $\mu\text{L}/\text{min}/\text{mg}$ in mouse, rat, and human liver microsomes, respectively. A similar tendency was found using hepatocytes from mice (133 $\mu\text{L}/\text{min}/10^6$ cells), rats (45 $\mu\text{L}/\text{min}/10^6$ cells), and humans (10 $\mu\text{L}/\text{min}/10^6$ cells). An in vitro screening assay using unlabeled (R)-YH134 showed no significant binding of the compound to any of the tested targets (Supplemental Table 2).

Radiochemistry and In Vitro Characterization

The enantiomerically pure *S*- or *R*-form of boronic ester was used as the precursor for copper-mediated radiofluorination to produce (S)- or (R)-[^{18}F]YH134. High radiochemical purity was achieved after semipreparative high-performance liquid chromatography purification (>99%). The molar activities of (R)-[^{18}F]YH134 were in the range of 102–277 GBq/ μmol at the end of the syntheses ($n = 13$). The distribution coefficient of (R)-[^{18}F]YH134 was

2.52 ± 0.18 ($n = 3$). No radioactive degradation products of (R)-[^{18}F]YH134 were observed in rodent or human plasma for up to 2 h (Supplemental Fig. 1). Its unbound fractions in rat and human plasma were $8\% \pm 1\%$ and $14\% \pm 2\%$, respectively ($n = 3$). (R)-[^{18}F]YH134 revealed a heterogeneous distribution in rat brain slices in in vitro autoradiography studies (Fig. 2A). The highest radioactivity accumulation appeared in the cortex, hippocampus, and striatum, regions known to express high levels of MAGL (29,30). Coincubation with MAGL inhibitors, either SAR127303 or PF-06809247, or with the reference compound (R)-YH134 substantially reduced the radioactive signal in the MAGL-rich brain regions. (R)-[^{18}F]YH134 demonstrated negligible binding in MAGL knockout mouse brain sections compared with that in wild-type mice (Fig. 2C, top). These results suggest high selectivity and specificity of (R)-[^{18}F]YH134 toward MAGL in vitro.

PET Scans and Biodistribution in MAGL Knockout and Wild-Type Mice

Figure 2B depicts the time–activity curves of PET scans of (R)-[^{18}F]YH134 and (S)-[^{18}F]YH134 in wild-type and MAGL knockout mice. As expected, (S)-[^{18}F]YH134, with modest MAGL half-maximal inhibitory concentrations, displayed no distinguishable differences between MAGL knockout and wild-type mice, whereas time–activity curves of (R)-[^{18}F]YH134 were substantially higher in wild-type than MAGL knockout mice over the whole scanning period (Fig. 2B). The significantly higher averaged SUV (1–91 min [SUV_{av}]) of (R)-[^{18}F]YH134 PET in wild-type than in MAGL knockout mice confirmed the high selectivity and specificity of (R)-[^{18}F]YH134 for MAGL in vivo (SUV_{av} , 0.84 ± 0.03 vs. 0.51 ± 0.02 ; $P < 0.001$). The representative sagittal and coronal PET images of (R)-[^{18}F]YH134 are in accordance with its in vitro autoradiography on wild-type and MAGL knockout mouse brain slices as shown in Figure 2C. To assess the whole-body distribution of radioactivity, we conducted biodistribution experiments after dissection of wild-type and MAGL knockout mice at 30 min after injection. The data

are summarized in Supplemental Table 3.

The radioactivity accumulation of (R)-[^{18}F]YH134 in MAGL knockout mouse brain was significantly lower than that in wild-type mice (1.31% vs. 1.75% injected dose/g, $P = 0.0225$). In the periphery, wild-type mice showed significantly higher radioactivity in a set of MAGL-expressing organs (2), such as the heart, brown adipose tissue, and adrenal gland. Regarding excretory pathways, radioactivity was high in both urine and bile.

In Vivo Metabolism and Plasma-to-Whole-Blood Ratio in Rats

The percentages of intact radiotracer in brain homogenates and plasma samples are summarized in Supplemental Table 4. Only intact radiotracer with a retention time of about 3.7 min was detected in mouse and rat brain homogenates up to 90 min after injection. In mouse plasma, a polar radiometabolite (retention time, 0.3 min) was detected at 45 and 90 min after injection. In contrast, the parental radiotracer remained the sole detectable

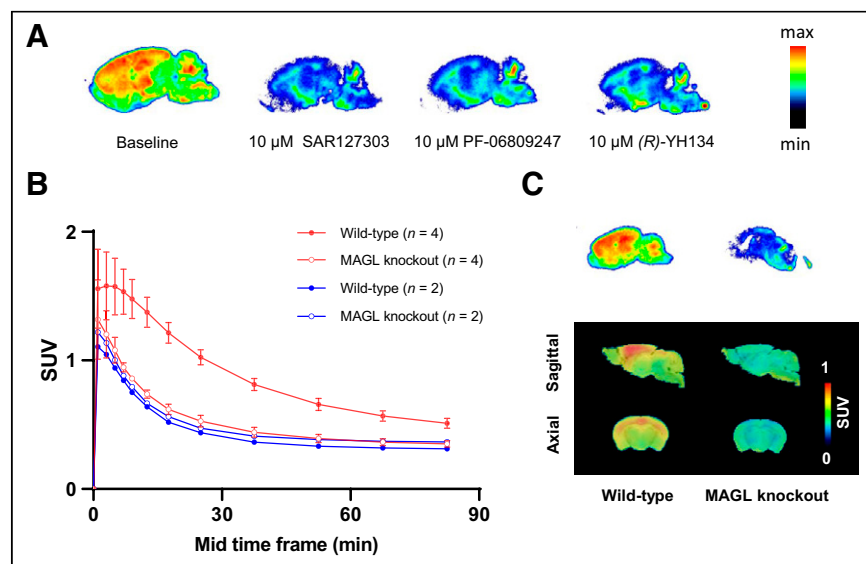


FIGURE 2. (A) In vitro autoradiography of (R)-[^{18}F]YH134 on rat brain sections. Baseline (13 nM (R)-[^{18}F]YH134 only) and blocking conditions are as indicated. (B) Brain time–activity curves of (R)-[^{18}F]YH134 (red) and (S)-[^{18}F]YH134 (blue) in MAGL knockout and wild-type mice. Mean values are given. Error bars indicate SD for $n = 4$. (C) In vitro autoradiograms (top) and in vivo brain PET images (bottom) of (R)-[^{18}F]YH134 averaged from 9.0 until 60 min after injection in wild-type and MAGL knockout mice. PET data are overlaid on MRI template.

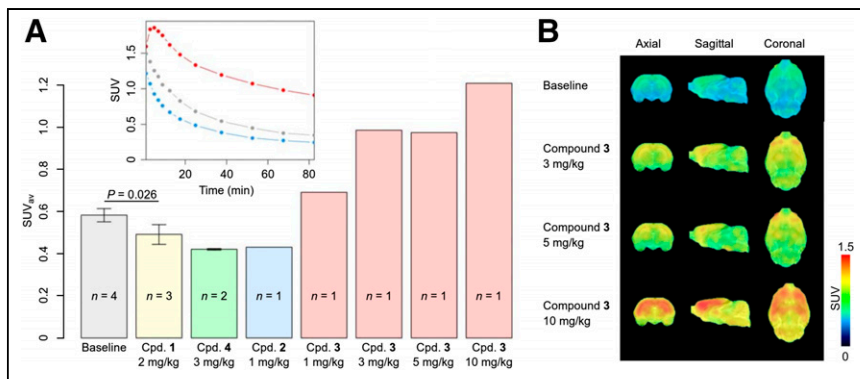


FIGURE 3. (A) SUV_{av} from PET brain time-activity curves of (R) - $[^{18}F]$ YH134 in Wistar rats under various blocking conditions. Significant blocking effect was revealed using compound **1** as blocker at 2 mg/kg ($P = 0.026$). Inset shows representative time-activity curves from baseline condition (gray), 1 mg/kg dose of compound **2** (blue), and 10 mg/kg dose of compound **3** (red). (B) Representative PET images of (R) - $[^{18}F]$ YH134 averaged from 8.0 to 90 min after injection with increasing doses of MAGL inhibitor **3**. Cpd. = compound.

radioactive species in rat plasma for up to 60 min after injection. Pretreatment with a 10 mg/kg dose of compound **3** did not alter the metabolic profile of (R) - $[^{18}F]$ YH134 in rat brain and blood. The plasma-to-whole-blood ratios in rats at defined time points under control and blockade conditions and their simulation with a biexponential function are shown in Supplemental Figure 2.

Effects of MAGL Blocking on (R) - $[^{18}F]$ YH134 PET in Rats

PET experiments were further performed on Wistar rats to evaluate the CNS binding of (R) - $[^{18}F]$ YH134 in the presence of the various MAGL drug candidates. The SUV_{av} calculated from PET brain time-activity curves is depicted in Figure 3A. Under blockade conditions with either MAGL inhibitor **1** or **2** (*19,21*), tracer accumulation in the brain was reduced, as expected for compounds competing with tracer binding to MAGL in rat brain. The blocking effect of a 2 mg/kg dose of compound **1** was significant, compared with the baseline SUV_{av} ($P = 0.026$). The presumably peripherally restricted MAGL inhibitor **4** containing a carboxylic acid group surprisingly reduced brain uptake of (R) - $[^{18}F]$ YH134 to the same level as for a 1 mg/kg dose of compound **2**. Pretreatment with compound **3**, a P-gp substrate with an efflux ratio of 7.65 (Supplemental Table 5), increased the SUV_{av} in a dose-dependent manner (1, 3, 5, and 10 mg/kg; Fig. 3A). Therefore, we selected compound **2** as a brain-penetrant blocker but compound **3** as a

peripherally restricted MAGL inhibitor for further kinetic studies. The respective PET images averaged from 8 to 90 min after injection are shown in Figure 3B.

Logan Plot and SUV_{av} Brain-to-Plasma Ratio to Quantify (R) - $[^{18}F]$ YH134 Distribution to Rat Brain

PET kinetic modeling with an IF was further performed to quantify brain uptake of (R) - $[^{18}F]$ YH134 and interpret the observed effects of compounds **2** and **3** on the brain SUV of (R) - $[^{18}F]$ YH134. Rats were injected with vehicle ($n = 3$), compound **2**, or compound **3** before tracer injection. (R) - $[^{18}F]$ YH134 brain uptake was analyzed by Logan plots of the PET data and the IF (V_T) and from the ratio between the SUV_{av} of brain and plasma (PET $SUV_{av}/IF\ SUV_{av}$). Representative Logan

plots are shown in Supplemental Figure 3.

In agreement with the previous section, compound **2** reduced the SUV_{av} of (R) - $[^{18}F]$ YH134 in rat brain. The effect of **2** (at 1 mg/kg) on brain uptake was significant (SUV_{av} at baseline, 0.560 ± 0.033 [$n = 3$], vs. SUV_{av} with **2**, 0.414 ± 0.036 [$n = 3$]; $P < 0.01$). The SUV_{av} of the IF was not reduced by compound **2** ($P = \sim 0.6$). However, the V_T and SUV_{av} brain-to-plasma ratios were significantly reduced by compound **2** (Figs. 4C and 4D), indicating significant competition between **2** and (R) - $[^{18}F]$ YH134 binding in rat brain. Administration of the peripheral blocker **3** (1–10 mg/kg) resulted in a significantly increased SUV_{av} in both brain and IF compared with baseline conditions (all doses included; $P < 0.0001$; Figs. 4A and 4B). However, the uptake-enhancing effect was cancelled out when V_T or SUV_{av} brain-to-plasma ratios were compared, in agreement with a lack of competition for MAGL binding in the brain.

Peripheral Target Occupancy Determined by (R) - $[^{18}F]$ YH134 PET

As concluded from the previous section, compound **3** enhanced (R) - $[^{18}F]$ YH134 SUV_{av} in rat brain and IF by occupying peripheral MAGL. We investigated whether we can estimate the dose of **3** at half-maximal MAGL blocking (D_{50}) in the periphery. Figure 5 shows the brain PET SUV_{av} and the IF SUV_{av} of plasma plotted

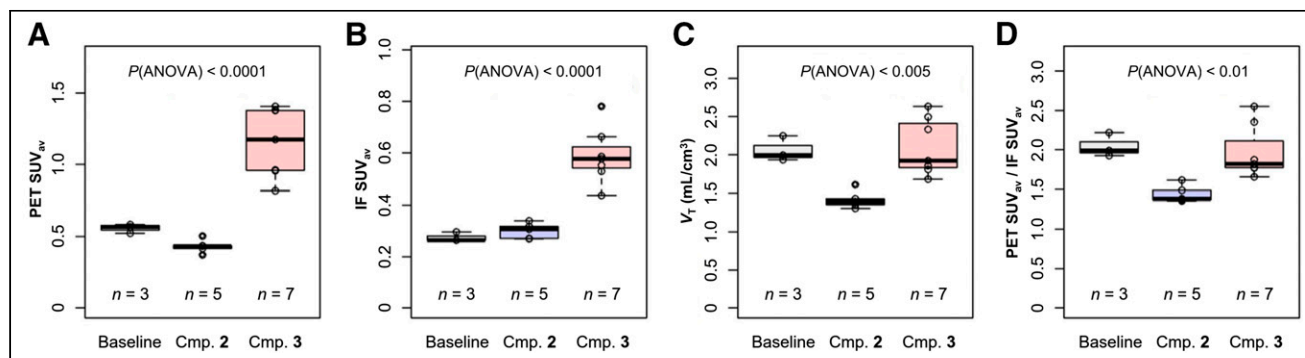


FIGURE 4. (A) (R) - $[^{18}F]$ YH134 SUV_{av} in rat brain. (B) (R) - $[^{18}F]$ YH134 SUV_{av} in rat plasma. (C) V_T in rat brain as determined by Logan plot analysis. (D) Ratio of SUV_{av} in rat brain and SUV_{av} in plasma. P values are shown for ANOVA. Injected doses of compounds **2** and **3** were neglected in this figure (doses are shown in Supplemental Table 1). Baseline = (R) - $[^{18}F]$ YH134 with vehicle; Cmp. **2** = blocking with compound **2** at doses from 1 to 3 mg/kg; Cmp. **3** = blocking with compound **3** at doses from 1 to 10 mg/kg.

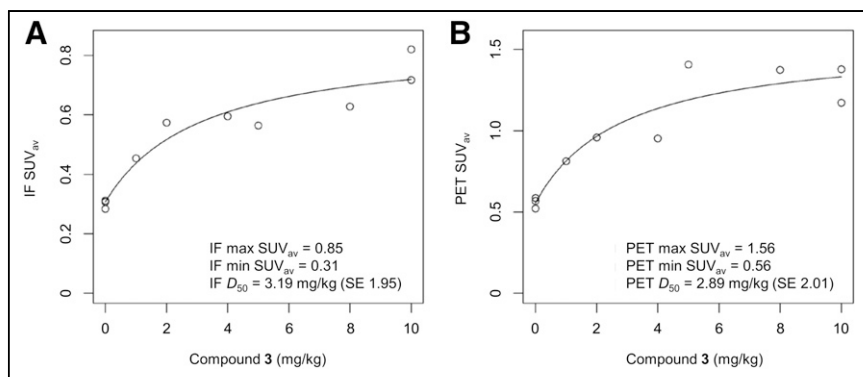


FIGURE 5. Peripheral MAGL occupancy by compound **3** determined with (*R*)-[¹⁸F]YH134. SUV_{av} in rat plasma (A, IF SUV_{av}) and brain (B, PET SUV_{av}) after injection of (*R*)-[¹⁸F]YH134 alone (0 mg/kg blocker) and after varying doses of compound **3** is indicated. Data were fit with 1:1 saturation function; fitted values are indicated in plots. Dose of (*R*)-[¹⁸F]YH134 at 0 mg/kg blocker was ~1 nmol/kg (<1 μg/kg).

against the blocker doses (same data as shown in Fig. 4). Analysis with a saturation function revealed D_{50} to be approximately 3 mg/kg in both cases. This is in line with the D_{50} of approximately 4 mg/kg estimated from the calculated percentage target occupancy at the averaged (0–100 min) plasma concentrations of **3**, back-calculated from the quantified plasma concentrations at 100 min at the various dose levels (Supplemental Fig. 4).

DISCUSSION

Moving the fluorine atom of (*R*)-YH149 from the *para*- to the *meta*-position of the phenyl ring resulted in (*R*)-YH134, with increased in vitro and in vivo stability. Our newly developed (*R*)-[¹⁸F]YH134 demonstrated increased MAGL in vivo specificity (Supplemental Fig. 5). Potential off-target binding of the tracer in mice was largely excluded on the basis of the low radioactive signal seen on in vitro autoradiography and in vivo PET studies on MAGL knockout mouse brain. These features suggest that (*R*)-[¹⁸F]YH134 is a promising MAGL PET tracer in rodents, and further studies on nonhuman primates are ongoing.

(*R*)-[¹⁸F]YH134 uptake in rat brain, expressed as V_T , SUV_{av}, or SUV_{av} ratio between brain and plasma, was significantly reduced by a 1 mg/kg dose of compound **2**, a potent MAGL brain-penetrant inhibitor (Supplemental Table 5). Compound **3**, a MAGL inhibitor with a high in vitro P-gp efflux ratio of 7.65 and therefore negligible distribution to the brain, affected brain SUV_{av} more than V_T or the SUV_{av} brain-to-plasma ratio. As for (*R*)-YH134, efflux ratios of 1.05 and 1.13 were obtained with mouse and human P-gp, respectively (Supplemental Table 5), indicating it is not a P-gp substrate. We therefore concluded that the radioactivity elevation in the brain was caused by blocking of peripheral MAGL binding sites rather than inhibition of P-gp-mediated efflux. The SUV_{av} brain-to-plasma ratio, because of its similarity to V_T determined with the Logan plot from PET data and IF, is a good surrogate for the V_T of (*R*)-[¹⁸F]YH134 in rat brain. Therefore, when MAGL in brain is targeted, tracer blood activity should be determined in addition to brain uptake. Our results, together with those of previous studies (31–33) on in vivo PET imaging of histone deacetylases and heat shock protein 90—targets expressed in both the CNS and the periphery—highlight the importance of normalization of radiotracer brain uptake to metabolite-corrected

plasma radiotracer levels to verify tracer-specific binding in blockade studies in vivo.

We further investigated whether our tracer can support the characterization of drug candidates targeting peripheral MAGL. The increasing brain uptake of (*R*)-[¹⁸F]YH134 in the presence of compound **3** was driven by the increased concentrations of free tracer in the blood. We therefore concluded that compound **3** bound mainly to peripheral MAGL, in agreement with its high P-gp efflux ratio determined in vitro. Indeed, the SUV_{av} of both brain and IF followed saturation functions, allowing fitting of D_{50} values for the saturation of peripheral MAGL by **3**. The result agrees with the D_{50} value obtained by measuring the plasma concentration

of **3** using the traditional method, liquid chromatography tandem mass spectrometry.

MAGL is not the only target expressed both in the CNS and in the periphery; this dual expression is also true for a variety of other targets, such as acetylcholine receptors (34), γ -aminobutyric acid receptors (35), heat shock protein 90 (33), and σ -receptors (36). Our current work demonstrates the utility of a CNS PET tracer in both brain and peripheral drug development. As whole-body PET scanners advance (37), a suitable PET tracer may help elucidate the complicated connections between the CNS and the periphery.

CONCLUSION

Our data suggest that (*R*)-[¹⁸F]YH134 is a promising PET tracer for noninvasive visualization and quantification of MAGL in pre-clinical studies. The V_T or SUV_{av} brain-to-plasma ratio of (*R*)-[¹⁸F]YH134 allows quantification of available MAGL binding sites in the brain, unaffected by peripheral MAGL blocking. Apart from being used to evaluate target engagement and the half-maximal MAGL occupancy of brain-penetrant MAGL inhibitors, (*R*)-[¹⁸F]YH134 brain PET can also be used to estimate the D_{50} of a peripherally restricted MAGL inhibitor. In our opinion, these promising preclinical results warrant the evaluation of (*R*)-[¹⁸F]YH134 as a MAGL PET tracer in a clinical setting. We believe that advances in whole-body PET scanners will enable a more comprehensive analysis of the endocannabinoid system under pathologic conditions or therapeutic intervention.

DISCLOSURE

This work was partially supported by the Swiss National Science Foundation (205321_192409/1). No other potential conflict of interest relevant to this article was reported.

ACKNOWLEDGMENTS

We sincerely thank Dr. Neil Parrott (Roche Innovation Center Basel) for fruitful discussions; Marie-Thérèse Miss, Isabelle Kaufmann, Roland Humm, Pawel Dzygiel, and Carina Cantrill (Roche Innovation Center Basel) for technical assistance; and Bruno Mancosu and Annette Krämer (ETH Zurich) for cyclotron support. Figdraw provided the material for the graphical abstract.

KEY POINTS

QUESTIONS: Is (R)-[¹⁸F]YH134 a suitable PET tracer for imaging MAGL in rodent brain? How does peripheral MAGL influence brain uptake of (R)-[¹⁸F]YH134 under blocking conditions?

PERTINENT FINDINGS: (R)-[¹⁸F]YH134 is a highly specific and selective PET tracer for MAGL brain imaging. V_T and SUV brain-to-plasma ratio are better suited than SUV to quantify MAGL binding in the brain under blocking conditions, and (R)-[¹⁸F]YH134 can be used to estimate the dose of MAGL inhibitor at half-maximal peripheral target occupancy.

IMPLICATIONS FOR PATIENT CARE: Our results warrant clinical translation of (R)-[¹⁸F]YH134. Clinical imaging of MAGL and advances in whole-body PET scanners will enable a more comprehensive analysis of the endocannabinoid system under pathologic conditions or therapeutic intervention.

REFERENCES

- Tornqvist H, Belfrage P. Purification and some properties of a monoacylglycerol hydrolyzing enzyme of rat adipose tissue. *J Biol Chem.* 1976;251:813–819.
- Karlsson M, Contreras JA, Hellman U, Tornqvist H, Holm C. cDNA cloning, tissue distribution, and identification of the catalytic triad of monoglyceride lipase. *J Biol Chem.* 1997;272:27218–27223.
- Nomura DK, Morrison BE, Blankman JL, et al. Endocannabinoid hydrolysis generates brain prostaglandins that promote neuroinflammation. *Science.* 2011;334:809–813.
- Piro JR, Benjamin DI, Duerr JM, et al. A dysregulated endocannabinoid-eicosanoid network supports pathogenesis in a mouse model of Alzheimer's disease. *Cell Rep.* 2012;1:617–623.
- Chen R, Zhang J, Wu Y, et al. Monoacylglycerol lipase is a therapeutic target for Alzheimer's disease. *Cell Rep.* 2012;2:1329–1339.
- Pasquarelli N, Porazik C, Bayer H, et al. Contrasting effects of selective MAGL and FAAH inhibition on dopamine depletion and GDNF expression in a chronic MPTP mouse model of Parkinson's disease. *Neurochem Int.* 2017;110:14–24.
- Hernández-Torres G, Cipriano M, Hedén E, et al. A reversible and selective inhibitor of monoacylglycerol lipase ameliorates multiple sclerosis. *Angew Chem Int Ed Engl.* 2014;53:13765–13770.
- Gil-Ordóñez A, Martín-Fontecha M, Ortega-Gutiérrez S, López-Rodríguez ML. Monoacylglycerol lipase (MAGL) as a promising therapeutic target. *Biochem Pharmacol.* 2018;157:18–32.
- Tuo W, Leleu-Chavaïn N, Spencer J, Sansook S, Millet R, Chavatte P. Therapeutic potential of fatty acid amide hydrolase, monoacylglycerol lipase, and N-acyl ethanolamine acid amidase inhibitors. *J Med Chem.* 2017;60:4–46.
- Fowler CJ. Monoacylglycerol lipase: a target for drug development? *Br J Pharmacol.* 2012;166:1568–1585.
- Blankman JL, Simon GM, Cravatt BF. A comprehensive profile of brain enzymes that hydrolyze the endocannabinoid 2-arachidonoylglycerol. *Chem Biol.* 2007;14:1347–1356.
- Nomura DK, Long JZ, Niessen S, Hoover HS, Ng SW, Cravatt BF. Monoacylglycerol lipase regulates a fatty acid network that promotes cancer pathogenesis. *Cell.* 2010;140:49–61.
- Matthews PM, Rabiner EA, Passchier J, Gunn RN. Positron emission tomography molecular imaging for drug development. *Br J Clin Pharmacol.* 2012;73:175–186.
- Lee C-M, Farde L. Using positron emission tomography to facilitate CNS drug development. *Trends Pharmacol Sci.* 2006;27:310–316.
- Phelps ME. Positron emission tomography provides molecular imaging of biological processes. *Proc Natl Acad Sci USA.* 2000;97:9226–9233.
- Takahata K, Seki C, Kimura Y, et al. First-in-human in vivo imaging and quantification of monoacylglycerol lipase in the brain: a PET study with ¹⁸F-T-401. *Eur J Nucl Med Mol Imaging.* 2022;49:3150–3161.
- Arakawa R, Takano A, Nag S, et al. Target occupancy study and whole-body dosimetry with a MAGL PET ligand [¹¹C]PF-06809247 in non-human primates. *EJNMMI Res.* 2022;12:13.
- He Y, Schild M, Grether U, et al. Development of high brain-penetrant and reversible monoacylglycerol lipase PET tracers for neuroimaging. *J Med Chem.* 2022;65:2191–2207.
- McAllister LA, Butler CR, Mente S, et al. Discovery of trifluoromethyl glycol carbamates as potent and selective covalent monoacylglycerol lipase (MAGL) inhibitors for treatment of neuroinflammation. *J Med Chem.* 2018;61:3008–3026.
- Grice CA, Buzard DJ, Shaghafi MB, inventors; Abide Therapeutics Inc., assignee. Magl inhibitors. Patent WO2019222266A1. November 21, 2019.
- Bell C, Benz J, Gobbi L, et al., inventors; Hoffmann-La Roche Inc., assignee. New heterocyclic compounds as monoacylglycerol lipase inhibitors. Patent WO2020035424A1. February 20, 2020.
- He Y, Gobbi LC, Herde AM, et al. Discovery, synthesis and evaluation of novel reversible monoacylglycerol lipase radioligands bearing a morpholine-3-one scaffold. *Nucl Med Biol.* 2022;108-109:24–32.
- Fischer H, Senn C, Ullah M, Cantrill C, Schuler F, Yu L. Calculation of an apical efflux ratio from P-glycoprotein (P-gp) in vitro transport experiments shows an improved correlation with in vivo cerebrospinal fluid measurements in rats: impact on P-gp screening and compound optimization. *J Pharmacol Exp Ther.* 2021;376:322–329.
- Bendels S, Bissantz C, Fasching B, et al. Safety screening in early drug discovery: an optimized assay panel. *J Pharmacol Toxicol Methods.* 2019;99:106609.
- Tredwell M, Preshlock SM, Taylor NJ, et al. A general copper-mediated nucleophilic ¹⁸F fluorination of arenes. *Angew Chem Int Ed Engl.* 2014;53:7751–7755.
- Goertzen AL, Bao Q, Bergeron M, et al. NEMA NU 4-2008 comparison of preclinical PET imaging systems. *J Nucl Med.* 2012;53:1300–1309.
- Müller Herde A, Keller C, Milicevic Sephton S, et al. Quantitative positron emission tomography of mGluR5 in rat brain with [¹⁸F]PSS232 at minimal invasiveness and reduced model complexity. *J Neurochem.* 2015;133:330–342.
- Logan J, Fowler JS, Volkow ND, et al. Graphical analysis of reversible radioligand binding from time-activity measurements applied to [¹¹C-methyl]-(-)-cocaine PET studies in human subjects. *J Cereb Blood Flow Metab.* 1990;10:740–747.
- Dinh TP, Carpenter D, Leslie FM, et al. Brain monoglyceride lipase participating in endocannabinoid inactivation. *Proc Natl Acad Sci USA.* 2002;99:10819–10824.
- Yamasaki T, Mori W, Zhang Y, et al. First demonstration of in vivo mapping for regional brain monoacylglycerol lipase using PET with [¹¹C]SAR127303. *Neuroimage.* 2018;176:313–320.
- Wang C, Schroeder FA, Wey HY, et al. In vivo imaging of histone deacetylases (HDACs) in the central nervous system and major peripheral organs. *J Med Chem.* 2014;57:7999–8009.
- Van de Bittner GC, Ricq EL, Hooker JM. A philosophy for CNS radiotracer design. *Acc Chem Res.* 2014;47:3127–3134.
- Vermeulen K, Cools R, Briard E, et al. Preclinical evaluation of [¹¹C]YC-72-AB85 for in vivo visualization of heat shock protein 90 in brain and cancer with positron emission tomography. *ACS Chem Neurosci.* 2021;12:3915–3927.
- Peralta EG, Ashkenazi A, Winslow JW, Smith DH, Ramachandran J, Capon DJ. Distinct primary structures, ligand-binding properties and tissue-specific expression of four human muscarinic acetylcholine receptors. *EMBO J.* 1987;6:3923–3929.
- Ben-Ari Y. Excitatory actions of gaba during development: the nature of the nurture. *Nat Rev Neurosci.* 2002;3:728–739.
- Rousseaux CG, Greene SF. Sigma receptors [σRs]: biology in normal and diseased states. *J Recept Signal Transduct Res.* 2016;36:327–388.
- Badawi RD, Shi H, Hu P, et al. First human imaging studies with the Explorer total-body PET scanner. *J Nucl Med.* 2019;60:299–303.